Effect of the Interfacial Transition Zone on ultrasonic wave attenuation and velocity in concrete

Manda Ramaniraka, Sandrine T. Rakotonarivo, Cédric Payan, Vincent Garnier

Keywords: characterization (B), Interfacial Transition Zone (B), concrete (E), ultrasound propagation

Effect of the Interfacial Transition Zone on ultrasonic wave attenuation and velocity in concrete.

Manda Ramaniraka*, Sandrine Rakotonarivo, Cédric Payan and Vincent Garnier

Aix Marseille Univ, CNRS, Centrale Marseille, LMA, Marseille, France

1. Introduction

Concrete constitutes the backbone of many existing infrastructures, from family houses to skyscraper, including bridge, highway and many more. A reliable diagnosis about its state of health is then crucial. Over the recent years, Non Destructive Evaluation (NDE) methods based on ultrasound propagation have shown great potentials [1]. However, ultrasound characterization of concrete structure remains a challenging task, mainly due to its complex microstructure that is very heterogeneous and random. Considering a short pulse input signal, the output signal recorded through such medium is much longer than the emitted signal. This time signal can be decomposed into two parts: (1) the early arrival times which corresponds to the wave propagating in an effective medium as if it is homogeneous, this wave is called the “ballistic wave” and (2) the latter arrival times which correspond to multiple wave paths inside the medium, this part is called “coda” [2]. After ensemble-averaging of time signals acquired over many realizations (i.e. different sensor positions on a concrete sample), ballistic wave from early arrival times builds up coherently to get the “coherent wave” whereas signal from the coda tends to zero due to the random and incoherent nature of the coda.

The coherent wave can be assimilated to a wave that propagates through an effective medium. This "homogenized medium" is dispersive and attenuating [4]. In other words, the effective velocity varies with frequency as well as the amplitude of the signal that is attenuated by the medium. Two main effective coherent parameters are thus mostly used to characterize concrete: the phase velocity and the attenuation [3] [4] [5] [6] [7]. The mechanical wave propagation velocity is directly linked to the mechanical properties of an elastic medium: Young modulus (E), Poisson's ratio (ν) and density (ρ) [10] [11]. It is thus used to assess evolutions of the mechanical properties of concrete [5] [6] [7]. On the other hand, the attenuation is noticed to be more sensitive to material's changes. In fact, two physical phenomena are at the origin of the wave attenuation trough the concrete: the multiple scattering of ultrasound by the aggregates and other possible scatterers (voids, cracks, etc.), and the absorption due to viscoelastic effects that are essentially in mortar [3] [4] [5] [6] [7].

The future of NDE lies on numerical simulations. In fact, they allow working with a controlled medium and they offer a multitude of possible configurations. Furthermore, it is much more cost-effective than working with a set of concrete samples from laboratory or extracted from the structure. "Numerical NDE" thus has become the indispensable help in the development process of a technique. The challenge is to reproduce as faithfully as possible the real-world wave-matter interactions in concrete, but in the simplest way. The simulated concrete is generally defined as a two-phase composite material composed of a mortar matrix containing aggregates inclusions. Until now, numerical ultrasound propagations in concrete were carried out assuming a perfect contact between those two phases [10] [11] [12]. In a physically sense, this assumption seems to be inaccurate. In fact, due to shearing stresses applied by the aggregate on the cement paste during mixing, water tends to be separated from the cement particles. This results in a thin layer

with more water around the aggregate, thus more porosity when concrete has set (Fig. 1). This is the well-known Interfacial Transition Zone (ITZ) [13] [14] [15] [16]. The smaller the aggregate, the smaller the ITZ: it can therefore be neglected for sand particles.

The results of numerical simulations carried out by [10] and [11], and our results considering perfect contact (section 2) at the aggregate/mortar interface, have shown a gap between the simulated coherent parameters and the experimental ones. Especially, about the attenuation, the experimental values are much higher. The aim of this study is to explain this gap through a realistic model which accounts for microstructural features. Two ways are explored: firstly, wrong estimations of the material properties defined in the simulation, which inevitably induce a bias on the impedance contrast, and secondly, the consideration of the ITZ at the aggregate/mortar interface. In fact, on the one hand, the impedance contrast between the scatterer and the matrix governs the scattering power of the medium [2]. And on the other hand, this multiple scattering of ultrasound is surely affected by the nature of the contact between them.

The study starts with an assessment of the variation of the numerical coherent parameters induced by a variation of the impedance contrast (section 2). Then it deals with the numerical modelling of the ITZ as an imperfect contact between the aggregate and the mortar (section 3). After that, the effects of such contact on the ultrasound scattering properties of one aggregate are quantified (section 4). Finally, considering many aggregates, the numerical coherent parameters obtained are presented (section 5), discussed and compared with experimental data.

2. The contribution of the impedance contrast variability

2.1. Attenuation: comparison between simulation and experiments

- **Description of the simulation**

A 2D numerical simulation considering perfect contact between the aggregates and the mortar was carried out at the first stage of the study (Fig. 1), with the properties given in Table. 1. The aggregates are randomly distributed monodisperse discs of 12mm in diameter with a surface density of 40%. The size of the computational domain is 40cmx25cm, including a 40cmx5cm band of mortar for incident wave initialization. The transmitted signal into the simulated concrete consists in a plane compressional wave, referred as P-wave throughout the manuscript, and a Ricker signal centered at 500kHz. Then, the wave propagates through the simulated concrete over 15cm. A grid of 31 (lines) by 16 (rows) receivers, i.e. a total of 496 receivers, are placed within the concrete specimen. The coherent signal $A_n(t, r_n)$, at receiver r_n in the grid, is obtained by an averaging over the 31 lines of receivers.

Table 1 : Simulated materials properties [10] [11] [12]

	Mortar	Aggregate
P-wave velocity (m/s)	3950	4300
S-wave velocity (m/s)	2250	2475
Density (kg/m^3)	2050	2610
Impedance contrast	1.39	

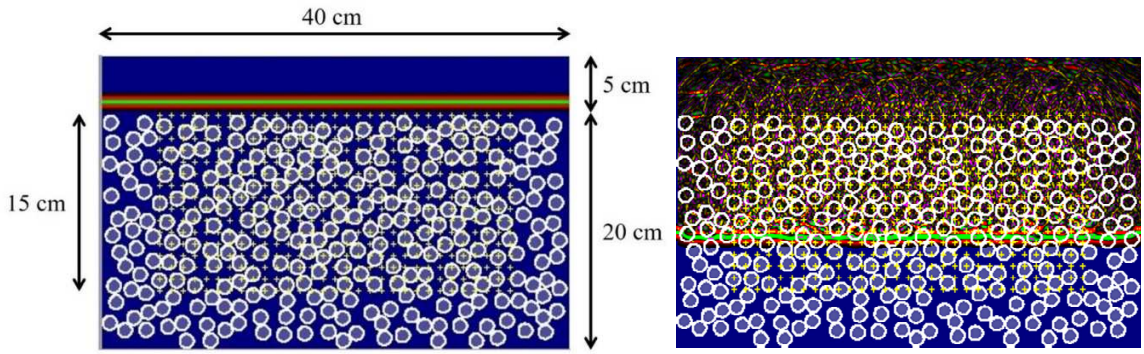

Figure 1 : Numerical simulation of wave propagation in concrete - snapshots at two different time steps; “green/red” color code = P-waves and “yellow/magenta” color code = S-waves; yellow points = receivers

- **Description of the attenuations**

Concerning experimental measurements: as mentioned in section 1, the attenuation of the coherent wave results from losses due to the multiple scattering by aggregates and the viscoelastic absorption in mortar. As the transducers used for measurements have a finite size, the beam divergence also contributes to the attenuation. The amplitude $A_n(f)$ of the coherent signal at receiver r_n and at the frequency f can be written as [3]:

$$A_n(f) = A(f, r_n) = A_0(f)e^{-(\alpha_s(f)+\alpha_a(f)+\alpha_d(f))r_n} \quad (1)$$

where $A_0(f)$ is the emitted amplitude; $\alpha_s(f)$, $\alpha_a(f)$ and $\alpha_d(f)$ the attenuations respectively from scattering, absorption and divergence.

Extensive studies about attenuation measurements were realized by Punurai et al [3] on cement paste specimens at high frequencies (2MHz and 5MHz), where scatterers are entrained air voids. Regarding the present numerical simulations: absorption was not considered, avoiding extra-time computing and allowing focusing on multiple scattering processes first, and a propagating plane wave avoided loss due to ultrasonic beam divergence. So, the attenuation is reduced to the only

contribution of the multiple scattering $\alpha(f) = \alpha_s(f)$. Its value is thus estimated by adjusting a regression line on the logarithmic decay of the amplitudes at increasing distances r_n. The numerical values of attenuation are plotted in Fig. 2 and are very similar to the numerical results performed in [10] and [11].

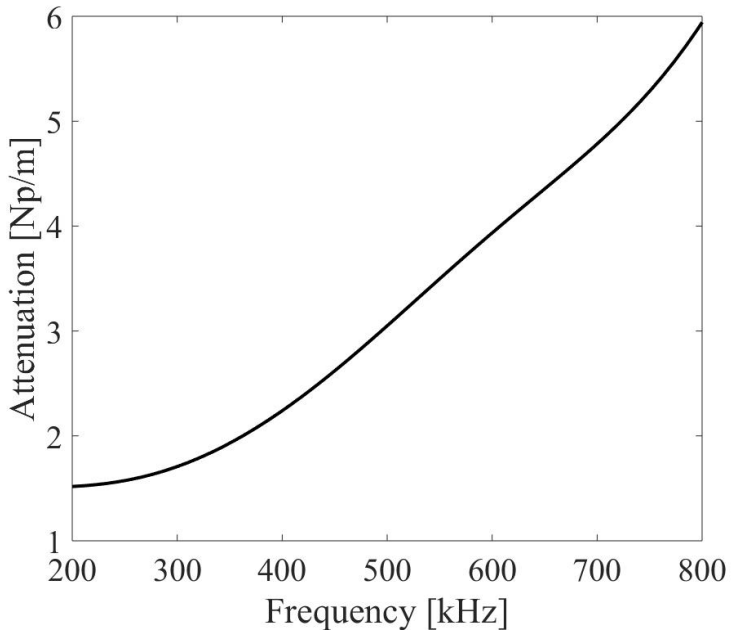

Figure 2 : Numerical attenuation with perfect contact

- **Comparison with the experimental attenuation values**

As a reminder, the study is focused on the multiple scattering process, which brings information about the material's microstructure. Consistent comparison between the attenuation values $\alpha_s(f)$ from the simulation (2D, no absorption and monodisperse circular aggregates) and those from experimental measurements (3D, absorption and polydisperse random shape aggregates) is possible for the following reasons:

- Theoretical calculations of attenuation for the case of incident P-wave, give the same value for 2D and 3D (with maximum deviation of 2Np/m) at the frequency bandwidth 400kHz-600 kHz [9].
- Ting et al [10] showed that aggregate shapes do not impact on the estimation of coherent parameters at this frequency range and for spatial random distributions, particularly the attenuation (with maximum deviation less than 0,2Np/m). Thus, simplified circular aggregates are considered in this paper.
- The case of polydisperse medium was not investigated in this study. But according to [9] [11], it smooths the coherent parameters frequency dependent curves.
- Thanks to attenuation measurements on mortar and/or cement paste samples in addition to concrete samples, the absorption contribution is subtracted from the total attenuation allowing to get the only multiple scattering contribution.

Some experimental values of P-wave attenuation at 500kHz from three different authors were collected (Table 2).

Table 2 : Experimental attenuation values

	Chaix et al. [8]	Chekroun et al. [9]	Philippidis et al. [7]
Total attenuation [Np/m]	31	24	38
Absorption contribution [Np/m]	9	7	26
Multiple scattering contribution [Np/m]	**22**	**17**	**12**

Those experimental values are clearly far from the numerical value of attenuation, which is about 3Np/m at 500kHz in the present simulation. Before investigating the effects of the nature of the contact at the mortar-aggregate interface, the study evaluates first the effects of simulated properties variability on the attenuation. In fact, multiple scattering of ultrasound is due to the impedance contrast between the mortar and the aggregates. The bigger the contrast, the more powerful the multiple scattering and the higher the attenuation.

2.2. Effects of the variation of the impedance contrast on the attenuation

Schubert et al. [12] discussed the variability of the mechanical properties of the concrete components. Starting with the values given in Table 1 as reference, they assumed that the mortar's properties are constant while the aggregate's properties vary as follows: P-wave velocity ±215m/s (±5%), S-wave velocity ±124m/s (±5%), and density ±130kg/m^3 (±5%).

As multiple scattering takes place due to aggregates stiffer than mortar, decreasing mechanical properties of aggregates will reduce the contrast and the attenuation. For the needs of this study, additional simulations were carried out with increasing values of contrasts: *the stiffness of the aggregates are gradually increased while the stiffness of the mortar decreased*. Three new simulated concrete are thus defined, with the same setup as in Figure 1 but with the mechanical properties given in Table 3.

Table 3 : Different simulated materials properties

	Ref+1		Ref+2		Ref+3	
	Mortar	Aggregate	Mortar	Aggregate	Mortar	Aggregate
P-wave [m/s]	3 895	4 390	3 840	4 480	3 785	4 570

S-wave [m/s]	2 245	2 547	2 240	2 620	2 235	2 692
Density [kg/m3]	2 025	2 619	2 000	2 628	1 975	2 637
Impedance contrast	1.46		1.53		1.61	

The impedance contrast of "Ref+3" is expressly exaggerated compared to the maximum contrast in [12] in order to highlight the limits of the variability's contribution in the attenuation. The numerical simulations give the following values of attenuation at 500kHz (Fig. 3):

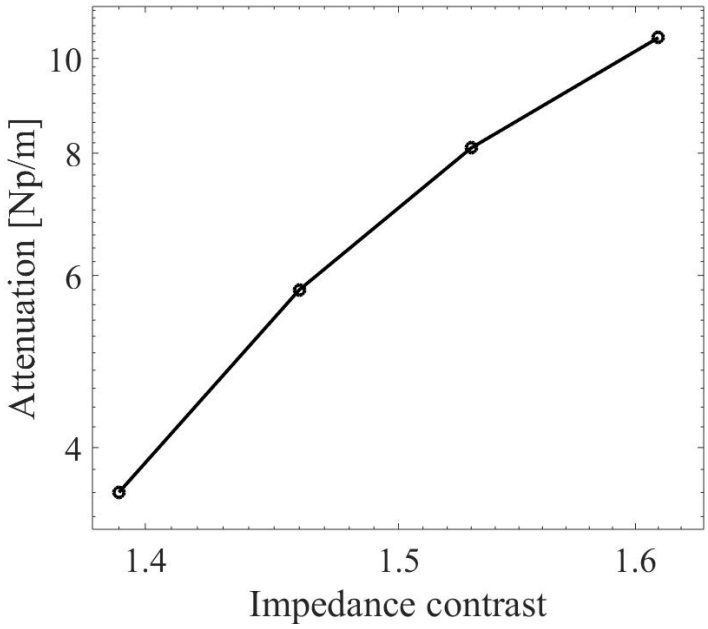

Figure 3: Numerical attenuation values for different contrasts at 500 kHz – x-and-y axis logarithmic scale

The results in Fig. 3 show that the maximum of attenuation that can be obtained, corresponding to the maximum of contrast (Ref+3), is about 10Np/m. A numerical simulation with the maximum contrast mentioned in [12] was also realized and produced an attenuation of 6Np/m. We note that the attenuation of max 10Np/m is still below the experimental attenuations given in Table 3 from [7], [8] and [9].

Thus, impedance variability cannot explain by itself alone the gap with the real-world measurements. Given the nature of the contacts between the aggregates and the mortar, an alternative explanation could be related to the Interfacial Transition Zone. Thus, modelling of ITZ and analysis of its effect on wave propagation is further explored in next sections.

3. Modelling of the Interfacial Transition Zone (ITZ)

3.1. About the ITZ

A large amount of studies has dealt with the description of ITZ [12] [13] [14] [15] [16]. It is commonly assumed that the interfacial zone has lower mechanical properties than the mortar bulk, due to its high porosity rate. It is also established that the ITZ governs concrete strength [14]. In fact, stress concentrations at this zone when the concrete is under loading are mostly the origin of cracks. This study has two points of interest: the thickness of ITZ and its mechanical properties (Young modulus and Poisson's ratio).

It is noticed that the thickness of the ITZ varies widely in the literature: from 10μm to 150μm [13]. The ITZ thickness depends on various parameters: the water/cement ratio, the surfaces of aggregates, the nature of cement, etc. If a thickness of 50μm is generally admitted for classical concrete [13] [14] [15], an ITZ of less than 10μm can be observed with Ultra High-Performance Concrete (UHPC) using fly ash [15]. Regarding the mechanical properties, the Poisson's ratio of ITZ is noticed to be the same as the Poisson's ratio of the mortar bulk, and the Young modulus of ITZ is ranging from 10 to 90% of the mortar bulk's Young modulus [15]. This brief review gives an idea of the variety of existing ITZ and brings to consider a simpler way to model this interface.

Modelling the ITZ as a thin layer around each aggregate in numerical simulations of ultrasound propagation would cost a tremendous time of computing. Jump conditions at aggregates-mortar

interfaces are good options. They avoid additional computing time and allow characterizing the ITZ with simple rheological parameters. It is already used in other fields as in geosciences and in glue bonding problems [17].

3.2. A "spring-mass" approach to model the ITZ

A rheological model consisting of a combination of normal and tangential linear springs and masses is used to model the imperfect contact. This approach was discretized and inserted into the 2D finite-difference-scheme-based software "Prospero" [17] [18]. It has been developed at the Laboratory of Mechanics and Acoustics (LMA, France) and used for all numerical simulations presented in this study. Comparisons with analytical solutions have shown the efficiency of this "spring-mass" approach [17].

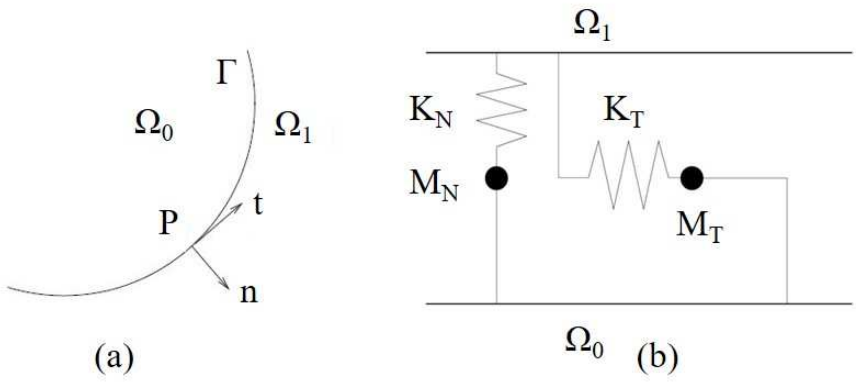

Figure 4: (a) Two elastic media Ω_0 and Ω_1 separated by an interface (Γ), P is a point at the interface, t and n are respectively the tangential and normal unit vectors;

(b) Spring-mass rheological model of the contact: $K_N > 0$, $K_T > 0$, $M_N \geq 0$ and $M_T \geq 0$ are respectively the normal stiffness, the tangential stiffness, the normal mass and the tangential mass of (Γ) [17];

The spring-mass conditions describing the jump conditions at the imperfect contact are:

$$[u_N(P,t)] = \frac{1}{K_N}\sigma_{N0}(P,t)\,; \quad [\sigma_N(P,t)] = M_N\frac{\partial^2}{\partial t^2}u_{N0}(P,t)$$

$$[u_T(P,t)] = \frac{1}{K_T}\sigma_{T0}(P,t)\,; \quad [\sigma_T(P,t)] = M_T\frac{\partial^2}{\partial t^2}u_{T0}(P,t) \qquad (2)$$

where $[u_N(P,t)]$, $[u_T(P,t)]$, $[\sigma_N(P,t)]$ and $[\sigma_T(P,t)]$ are respectively the normal displacement, the tangential displacement, the normal stress and the tangential stress jumps across the interface (Γ) at the point P and at time t, from Ω_0 to Ω_1;

It is a simplified way to describe a wide range of contacts, from perfect bonding to stress-free surfaces. In fact, one has just to tune the stiffness and mass values. For the perfect contact case, (2) becomes:

$$[u_N(P,t)] = 0\,; \quad [\sigma_N(P,t)] = 0$$

$$[u_T(P,t)] = 0\,; \quad [\sigma_T(P,t)] = 0 \qquad (3)$$

Readers are invited to refer to [18] for more details about the software "Prospero" and the numerical implementation of imperfect contacts. The conditions (2) are already widely used for glue bonding control problems. Generally, the stiffnesses and the masses are defined as [17]:

$$K_N = \frac{\bar{\lambda}+2\bar{\mu}}{\bar{h}};\ K_T = \frac{\bar{\mu}}{\bar{h}};\ M_N = 0;\ M_T = 0 \qquad (4)$$

where $\bar{h}$ is the thickness and $\bar{\lambda}, \bar{\mu}$ the Lamé's coefficients of the "intermediate" elastic medium between Ω_0 (=aggregate) and Ω_1 (=mortar). $\bar{h}$ is small enough compared to other dimensions so that masses are neglected.

For an application on concrete, as said in section 3.1, the thicknesses and the moduli of the ITZ vary widely making it critical to assign specific values of ITZ thickness and physical parameters

(Lamé coefficient or Young modulus). To overcome this difficulty, the following parameter CL, for "Contact Level", was defined in order to have just one variable describing the contact between the aggregate and the mortar.

$$CL = \frac{E(ITZ)/E(mortar)}{\bar{h}} \tag{5}$$

Assuming that the Poisson ratio is the same for the ITZ and for the mortar [15] and introducing the CL's expression in the spring and mass formulations, (4) yields

$$K_N = CL \times \rho_0 {C_0^P}^2;\ K_T = CL \times \rho_0 {C_0^S}^2;\ M_N = 0;\ M_T = 0 \tag{6}$$

where ρ_0, C_0^P and C_0^S are respectively the density, the P-wave velocity and the S-wave velocity in the mortar [10] [11] [12].

4. ITZ effects on one aggregate

Numerical simulations were carried out to take into account different values of CL in order to study the effects of an imperfect contact on the scattering properties of one aggregate:

- $CL = +\infty$ (perfect contact)
- $CL \in [500\text{m}^{-1},\ 18500\text{m}^{-1}]$
- $CL = 0$ (fully debonded)

For better interpretation of those values, let's consider the ITZ thickness and let's remind that values of the ITZ's Young modulus range from 10 to 90% of the mortar bulk's Young modulus [15]. Variation of the single parameter CL can be interpreted as either a variation of the ITZ thickness and/or a variation of its modulus. However, at this stage of the study and in order to limit the number of variables, the ITZ modulus value is supposed to be constant at 10% of the

mortar's modulus. Such value was chosen because it allows obtaining a corresponding ITZ thickness in agreement with ITZ thicknesses found in the literature [14] [15] [16]. The correspondence between CL values and ITZ thicknesses for an ITZ Young modulus of 10% of the mortar's Young modulus is summarized in Table 4:

Table 4 : Correspondence between CL values and ITZ thicknesses

(considering an ITZ modulus of 10% of the mortar's Young modulus)

CL [m^{-1}]	500	1500	2500	3500	4500	5500	6500	7500	8500	9500
ITZ thickness [µm]	200,0	66,7	40,0	28,6	22,2	18,2	15,4	13,3	11,8	10,5

CL [m^{-1}]	10500	11500	12500	13500	14500	15500	16500	17500	18500	Inf.
ITZ thickness [µm]	9,5	8,7	8,0	7,4	6,9	6,5	6,1	5,7	5,4	0

The simulations consisted of incident plane waves (P-wave and S-wave) on an aggregate with materials properties given in Table 1. The emitted signal was a Ricker centered at 500kHz. A ring of receivers was placed around it to record diffracted waves from all directions. This basic setup is very practical for scattering problems: it allows to study how the wave is scattered by an obstacle and to quantify the "scattering power" of this obstacle.

Two parameters are usually used to characterize this scattering power [2]: the differential scattering cross section, which is the angular distribution of the ratio between the scattered wave and the incident wave ("angular scattering power"), and the total scattering cross section, which is calculated by angular integration of the differential scattering cross section ("total scattering power").

4.1. Differential scattering cross section σ_d

The differential scattering cross section σ_d depends on the six parameters listed in Table 1. The latter is then a function of the physical properties of the matrix and of the scatterer, and is frequency dependent. Its calculation is based on the boundary conditions between those two phases. Diffracted P-wave and S-wave are considered for each incident wave type, allowing to have the scattering cross sections without and with mode conversion (an incident P-wave giving a diffracted S-wave and vice versa).

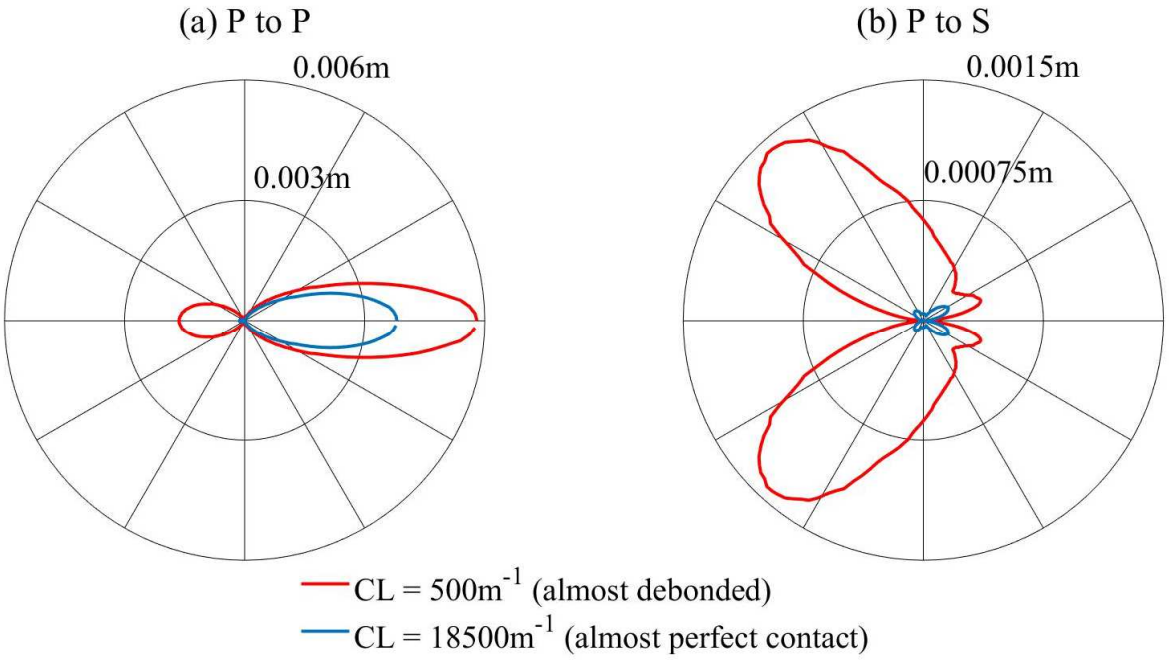

Figure 5 : An example of comparison between the differential scattering cross sections for two different levels of contact – Incident P-wave: (a) no mode conversion; (b) mode conversion

Fig. 5 shows an example of comparison between two different levels of contact for an incident P-wave: $CL = 18500\text{m}^{-1}$, which tends to a perfect contact and $CL = 500\text{m}^{-1}$, which tends to a debonding.

- For the P to P component (Fig. 5(a)), diffraction happens without mode conversion: the two differential cross sections have the same shape. However, the forward diffraction is more pronounced with the almost debonded case, meaning that more energy is diffracted in the forward direction for low bonding case.
- For the P to S component (Fig. 5(b)), diffraction happens with mode conversion: the two curves are completely different. Globally, the scattering power is much higher when the contact tends to a debonding. In addition to this, the two backward side lobes are more pronounced with the almost debonded contact while it is the case of the two forward side lobes with the almost perfect contact.

This simulation shows that the nature of the contact between the aggregate and the mortar strongly impacts ultrasound scattering by the aggregate. The total scattering cross section is then calculated to estimate the "total scattering power" of this aggregate.

4.2. Total scattering cross sections σ_t

The total scattering cross sections are calculated by the integration of the differential scattering cross sections over all directions θ:

$$\sigma_t = \int_0^{2\pi} \sigma_d(\theta) d\theta \quad (7)$$

It is a characteristic variable for scattering problems: in optics, in nuclear physics or in acoustics. It quantifies energy of the scattered wave by an object solicited by an incident wave. The evolution of this "total scattering power" according to the level of contact is shown in Fig. 6. From a perfect contact to a complete debonding, a minimum of the scattering cross sections curves is noticed around $CL = 1000\text{m}^{-1}$, except for the P→S component whose meaning investigation is still ongoing. This shape of the curves could be interpreted as an inversion of the

impedance contrast between the mortar and the aggregate as the contact is altered. The maximum values are obtained for $CL = 0\mathrm{m}^{-1}$, corresponding to a complete debonding.

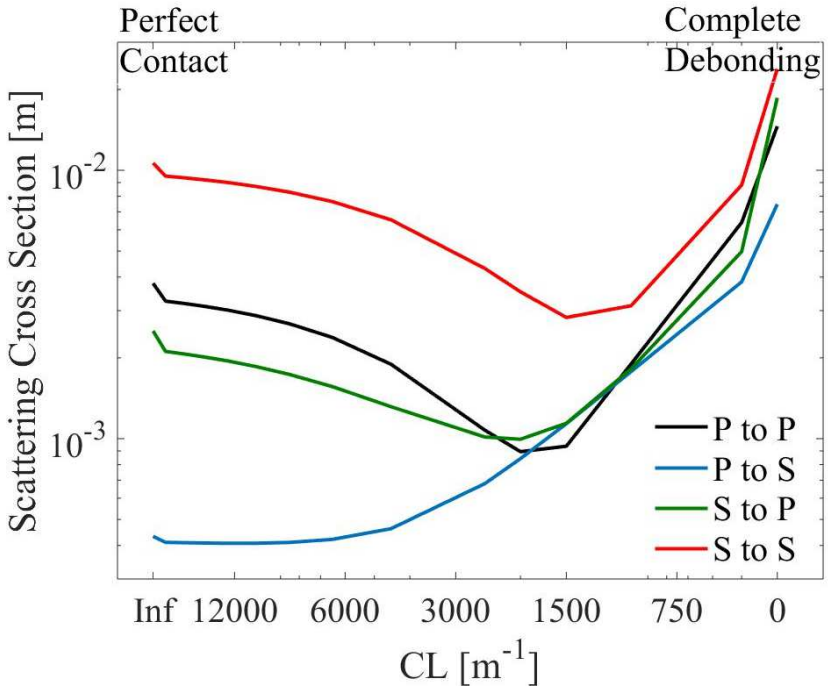

Figure 6 : Evolution of the scattering section as a function of the parameter CL : from a perfect contact to a complete debonding – x-and-y axis logarithmic scale

Calculating the total scattering cross section was important in order to check the effects of imperfect contact on ultrasound scattering by an aggregate. In the case of many aggregates, as it is the case in concrete, this scattering cross section is assumed to be directly linked to the attenuation of the coherent wave [10] [11]. Many theoretical models of homogenization exist and make link between the scattering cross section of an aggregate and the attenuation through the scattering medium [10] [11]. The higher the scattering cross section, the higher the attenuation.

It is important to know where in the curve (Fig. 6) is the case of real-world concrete. It is on the increasing part. As mentioned in section 3.1, ITZ is the “weak-link” of concrete due to its high porosity. So, damages applied to concrete (chemical or mechanical or thermal) impact firstly and

essentially the ITZ. A higher level of damage leads thus to a lower level of contact between the aggregate and the mortar. The analysis of experimental measurements on concrete samples with increasing damages shows a growth of the scattering power [4]. That confirms that a real concrete would be located on the increasing part.

5. ITZ effects for an ensemble of aggregates

The same numerical simulations as in section 2 were carried out with different values of CL ranging from 250m^{-1} to 2750m^{-1}, that means around the minimum of the curve in Fig. 7 and the increasing part. These values of CL correspond to ITZ thicknesses ranging from 35µm to 400µm when considering a Young modulus of the ITZ of 10% of the mortar's Young modulus. As a reminder, studies about ITZ characterization have shown thicknesses between 10µm and 150µm [14] [15]. The "Ref+2" in Table 3 is chosen for the simulation because it integrates an attenuation from the impedance contrast (8Np/m, Fig. 1) that could be the case with a real-world concrete.

5.1. Attenuation

Fig. 7 shows the evolution of the attenuation for decreasing values of the CL. At the beginning, when considering perfect contacts at aggregates/mortar interfaces, the attenuation is about 8Np/m. Then, a slight trough of the attenuation curve is observed at $CL = 2750\mathrm{m}^{-1}$. Therefatter, a monotonic growth of the attenuation curve is noticed as the contact level is decreasing. The attenuation value reached more than 50Np/m at $CL = 250\mathrm{m}^{-1}$.

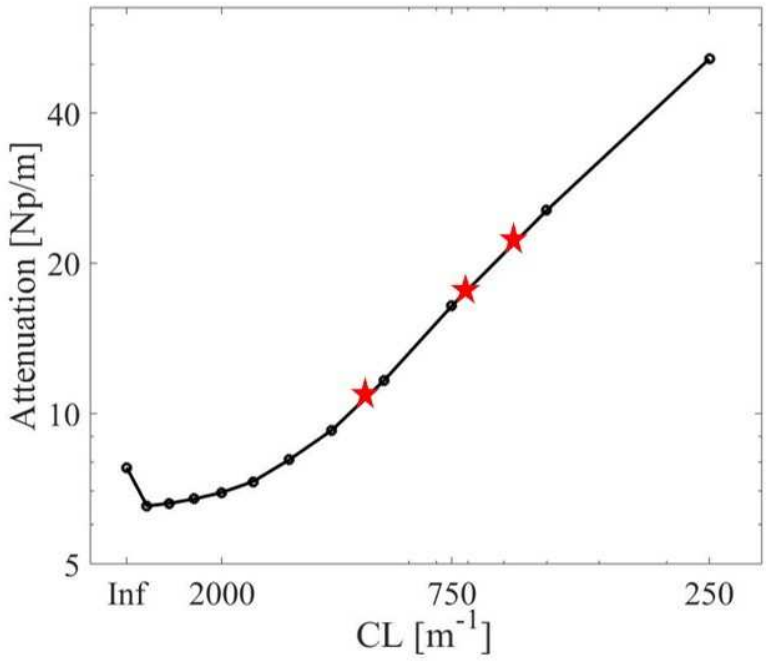

Figure 7 : P-wave attenuations obtained from numerical simulations for different levels of contact - at 500kHz – x-and-y axis logarithmic scale; red stars = experimental values of attenuation (11Np/m, 17Np/m, 22Np/m in Table 2)

5.2. Effective velocity

The effective velocity can be easily calculated by the ratio between a known distance of propagation and the arrival time of the computed coherent wave [10] [11]. The 11th range of receivers, corresponding to a distance of 10cm (Fig. 1), is chosen to estimate the velocity. This is a good compromise between a sufficient distance of propagation and a sufficient wave amplitude at reception. In Fig. 8, the velocity decreases as the level of contact decreases. This trend is in agreement with the following: an altered contact between aggregate and mortar, corresponding to a weaker ITZ, softens the material. It is interesting to notice that no coherent wave survived for a complete debonding case.

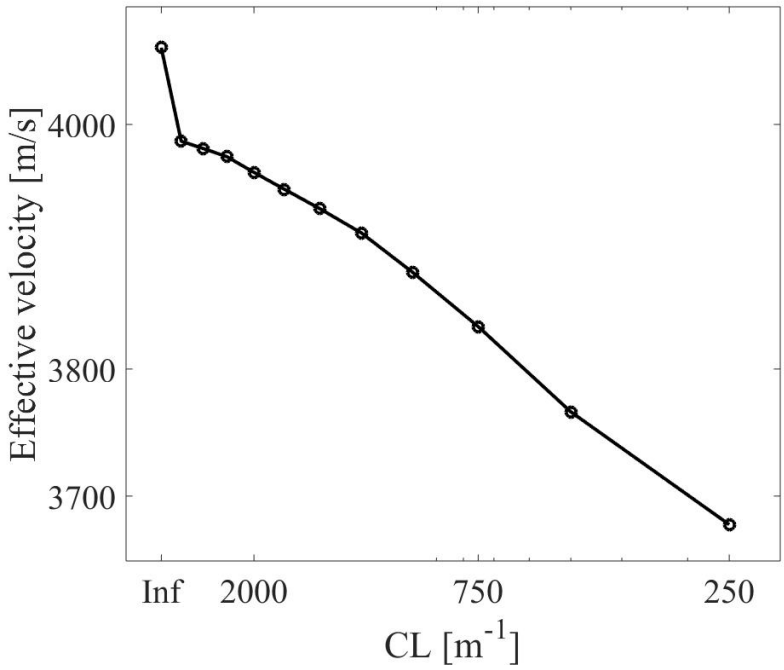

Figure 8 : P-wave velocities obtained from numerical simulations for different levels of contact – at 500kHz – x-and-y axis logarithmic scale

6. Discussions

From the main results in sections 3, 4 and 5, it is shown that firstly the impedance contrast is not able to explain the gap between the experimental and numerical data and secondly that the ITZ in numerical simulations impacts considerably the results, either for one aggregate or for an ensemble of aggregates. Now, it is important to link those results to the experimental results.

6.1. About the attenuation

As a reminder, this study aims to explain the gap noticed between numerical simulations (about 3Np/m) and the experiments regarding the coherent parameters estimation (about 17Np/m). In section 2, it was showed that even a maximum of impedance contrast could not explain

completely the bias of the attenuation values. The maximum gap that we can corrected through the variability of the material is close to 10Np/m.

The experimental multiple scattering attenuations in Table 2 are positioned on the numerical attenuation curve in Fig. 7 (red stars). After a projection on the abscissa axis, they correspond respectively to CL values of approximatively 600m^{-1}, 725m^{-1} and 1100m^{-1}. Finally, using Eq. (5) and considering an ITZ modulus of 10% of the mortar's Young modulus, those values correspond respectively to ITZ thicknesses of 165µm, 135µm and 90µm. They are in the order of magnitude found in the literature and described in section 3.

So, taking ITZ into account in numerical simulations, through imperfect contacts, enables to complete the explanation of the observed gap between the numerical and the experimental attenuations. The only variability of the simulated materials, involving only the impedance contrast, was not enough to explain this gap.

6.2. About the effective velocity

As the physical properties of the simulated concrete (wave velocities in Table 3) are not exactly the same as of the experimental concrete samples ([7] [8] [9]), quantitative comparison is not addressed. However, the trend observed in the numerical results (Fig. 8) is confirmed by the experimental velocity measurements for different levels of thermal damage on concrete samples: the measured velocity decreases as the thermal damage increases (Fig. 9) [8]. This increasing thermal damage alters the ITZ, which is the weak link of the concrete. That decreases the contact level at aggregates/mortar interfaces and thereby the velocity of the propagating wave. The next step would be to link a specific level of damage to a specific level of contact to estimate a value of CL. This study allowed thus a relative comparison on the effective velocity values (Fig. 9).

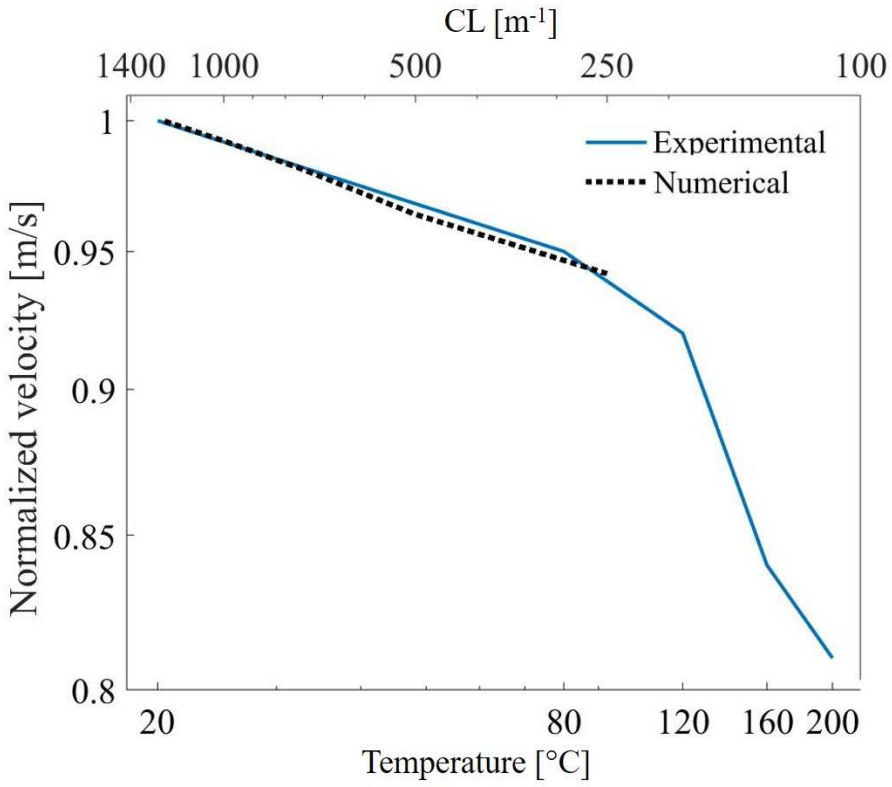

Figure 9: solid blue line = measured velocities for different level of thermal damages (lower X-axis) normalized by the undamaged value [8] ; dotted black line = velocities from simulations for different level of CL (upper X-axis) normalized by an assumed undamaged value ($CL = 1250m^{-1}$) – x-and-y axis logarithmic scale

7. Conclusion

The present study shows the major influence of the ITZ on ultrasonic measurements in concrete. This study quantitatively explains the gap noticed in the literature between the attenuation values from simulations (about 3Np/m) and experiments (about 20Np/m). The two main reasons are found to be: the variability of the impedance contrast, and the consideration of the ITZ in numerical simulations. The approach developed in this paper is an imperfect contact modeled through a spring mass system accounting for the physical parameters of the ITZ. The validation is performed using data from thermally damaged samples known to affect the ITZ. This new

approach allows a quantitative comparison between the attenuation values from the numerical simulations and experimental data as well as a relative comparison between the velocities. It is worth noticing that the present approach provides reliable means to address early detection of Alkali Silica Reaction (ASR) or Delayed Ettringite Formation (DEF) which drastically changes ITZ properties. Future work will address the inverse problem in order to provide a reliable damage indicator from the measured coherent ultrasonic parameters based on this numerical forward model.

Acknowledgements

The authors thank B. Lombard (Aix Marseille Univ, CNRS, Centrale Marseille, LMA, Marseille, France) for helpful discussions and providing « Prospero » software.

References

[1] J.-P. Balayssac, V. Garnier, Non-destructive Testing and Evaluation of Civil Engineering Structures", first ed., ISTE Press, France, 2017

[2] A. Derode, A. Tourin, M.Fink, Random multiple scattering of ultrasound. I. Coherent and ballistic waves", Physical Review E 64 (2001)

[3] W. Punurai, J. Jarzynski, J. Qu, J.-Y. Kim, L. Jacobs, K. Kurtis, Characterization of multi-scale porosity in cement paste by advanced ultrasonic techniques, Cement and Concrete Research 37 (2007) 38-46

[4] F. Saint-Pierre, P. Rivard, G. Ballivy, Measurement of alkali-silica reaction progression by ultrasonic waves attenuation, Cement and Concrete Research 37 (2007) 948-956

[5] Z. Lafhaj, M. Goueygou, A. Djerbi, M. Kaczmarek, Correlation between porosity, permeability and ultrasonic parameters of mortar with variable water/cement ratio and water content, Cement and Concrete Research 36 (2006) 625-633

[6] L. Vergara, R. Miralles, J. Gosalbez, F.J. Juanes, L.G. Ullate, J.J. Anaya, M.G. Hernandez, M.A.G Izquierdo, NDE ultrasonic methods to characterize the porosity of mortar, NDT&E International 34 (2001) 557-562

[7] T.P. Philippidis, D.G. Aggelis, Experimental study of wave dispersion and attenuation in concrete, Ultrasonics 43 (2005) 584-595

[8] J.-F. Chaix, Caractérisation non destructive de l'endommagement de bétons. Apport de la multidiffusion ultrasonore, PhD thesis, Université de la Méditerranée, 2003

[9] M. Chekroun, "Caractérisation mécanique des premiers centimètres du béton avec des ondes de surface", PhD thesis, Ecole Centrale de Nantes, 2008

[10] T. Yu, J.-F Chaix, L. Audibert, D. Komatitsch, V. Garnier, J.-M. Hénault, Simulations of ultrasonic wave propagation in concrete based on a two-dimensional numerical model validated analytically and experimentally, Ultrasonics 92 (2019) 21-34

[11] M. Chekroun, L. Le Marrec, B. Lombard, J. Piraux, Time-domain numerical simulations of multiple scattering to extract elastic effective wavenumbers, Waves in Random and Complex Media 22 (2012) 398-422

[12] F. Schubert, B. Koehler, Numerical time-domain simulation of diffusive ultrasound in concrete, Ultrasonics 42 (2004) 781-786

[13] G. Prokopski, J. Halbiniak, Interfacial transition zone in cementitious materials, Cement and Concrete Research 30 (2000) 579-583

[14] M. Königsberger, M. Hlobil, B. Delsaute, S. Staquet, C. Hellmich, B. Pichler, Hydrate failure in ITZ governs concrete strength: A micro-to-macro validated engineering mechanics model, Cement and Concrete Research 103 (2018) 77-94

[15] D. Keinde, S. Kamali-Bernard, F. Bernard, I. Cisse, Effect of the interfacial transition zone and the nature of the matrix-aggregate interface on the overall elastic behavior of concrete under compression: a 3D numerical study, European Journal of Environmental and Civil Engineering 18 (2014) 1167-1176

[16] G. Bonifazi, G. Capobianco, S. Serranti, M. Eggimann, E. Wagner, F. Di Maio, S. Lotfi, The ITZ in concrete with natural and recycled aggregates: Study of microstructures based on image and SEM analysis, 15th Euroseminar on Microscopy Applied to Building Materials, 17-19 June 2015, Delft, The Netherlands

[17] B. Lombard, J. Piraux, Numerical modeling of elastic waves across imperfect contacts, Society for Industrial and Applied Mathematics 28 (2006) 172-205

[18] B. Lombard, Modélisation numérique de la Propagation et de la Diffraction d'Ondes Mécaniques, HDR thesis, Université de la Méditerranée, 2010